ACS AuthorChoice

Environmental Science & Technology Letters

Letter

pubs.acs.org/journal/estlcu

Uranium(V) Incorporation Mechanisms and Stability in Fe(II)/Fe(III) (oxyhydr)Oxides

Hannah E. Roberts,[†] Katherine Morris,[†] Gareth T. W. Law,[†,‡] J. Frederick W. Mosselmans,[§] Pieter Bots,[†,#] Kristina Kvashnina,[∥,⊥] and Samuel Shaw*[,†]

[†]Research Centre for Radwaste Disposal and Williamson Research Centre for Molecular Environmental Science, School of Earth and Environmental Sciences, The University of Manchester, Manchester M13 9PL, United Kingdom

[‡]Centre for Radiochemistry Research, School of Chemistry, The University of Manchester, Manchester M13 9PL, United Kingdom

[§]Diamond Light Source Ltd., Diamond House, Harwell Science and Innovation Campus, Didcot, Oxfordshire OX11 0DE, United Kingdom

[∥]The Rossendorf Beamline at ESRF-The European Synchrotron, CS40220, 38043 Grenoble Cedex 9, France

[⊥]Helmholtz Zentrum Dresden-Rossendorf (HZDR), Institute of Resource Ecology, P.O. Box 510119, 01314 Dresden, Germany

Supporting Information

ABSTRACT: Understanding interactions between radionuclides and mineral phases underpins site environmental cleanup and waste management in the nuclear industry. The transport and fate of radionuclides in many subsurface environments are controlled by adsorption, redox, and mineral incorporation processes. Interactions of iron (oxyhydr)oxides with uranium have been extensively studied because of the abundance of uranium as an environmental contaminant and the ubiquity of iron (oxyhydr)oxides in engineered and natural environments. Despite this, detailed mechanistic information regarding the incorporation of uranium into Fe(II)-bearing magnetite and green rust is sparse. Here, we present a co-precipitation study in which U(VI) was reacted with environmentally relevant iron(II/III) (oxyhydr)oxide mineral phases. On the basis of diffraction, microscopic, dissolution, and spectroscopic evidence, we show the reduction of U(VI) to U(V) and stabilization of the U(V) by incorporation within the near surface and bulk of the particles during co-precipitation with iron (oxyhydr)oxides. U(V) was stable in both magnetite and green rust structures and incorporated via substitution for octahedrally coordinated Fe in a uranate-like coordination environment. As the Fe(II)/Fe(III) ratio increased, a proportion of U(IV) was also precipitated as surface-associated UO_2. These novel observations have significant implications for the behavior of uranium within engineered and natural environments.

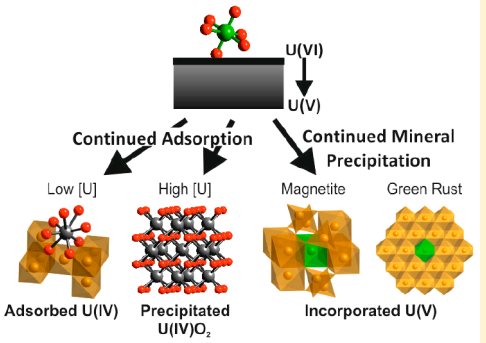

INTRODUCTION

Uranium is a problematic contaminant at nuclear sites and is the dominant radionuclide by mass in radioactive wastes destined for geological disposal. Groundwater conditions under both scenarios range from mildly acidic to alkaline and from oxic to anoxic.[1−4] The oxidation state of uranium significantly controls its mobility. Under oxic conditions, soluble and environmentally mobile U(VI) dominates; under anaerobic conditions, uranium is typically reduced to poorly soluble U(IV). During biological and abiotic reduction of U(VI), U(V) reportedly forms as a transient species.[5−7] Recent work has also suggested that U(V) can be stabilized at mineral surfaces[8−12] and via incorporation into environmentally relevant iron (oxyhydr)oxide phases such as goethite (α-FeOOH) and magnetite ($Fe^{II}Fe^{III}_2O_4$).[13−21] Indeed, establishing the extent of U(V) stability upon interaction with Fe (oxyhydr)oxides is essential in underpinning predictive models for U behavior in environmental systems that currently do not recognize the presence of U(V). To achieve this, U speciation needs to be determined at a molecular scale, which is a key step in defining the significance of U(V) in environmental systems and in developing realistic models for predicting the environmental fate of uranium.

Fe(II)/Fe(III)-bearing (oxyhydr)oxide minerals such as magnetite and green rust[22] (e.g., $[Fe^{II}_3Fe^{III}(OH)_8]^+[Cl,nH_2O]^-$) are ubiquitous in anoxic subsurface environments (e.g., soils and sediments), forming via a variety of biogeochemical processes[23,24] and during the anaerobic corrosion of steel, a significant component in contaminated, engineered environments and geological disposal facilities.[25−27] Recent studies have suggested possible pathways for how U(VI) reduction occurs at the magnetite surface.[8,10,11,28] Some studies suggest U(VI) is reduced to directly

Received: August 16, 2017
Revised: September 6, 2017
Accepted: September 8, 2017
Published: September 8, 2017

DOI: 10.1021/acs.estlett.7b00348
Environ. Sci. Technol. Lett. XXXX, XXX, XXX−XXX

form U(IV),[29] whereas other studies show U(VI) is reduced to U(V) via a one-electron transfer process and then U(V) disproportionates to form U(IV).[28,30] Previous spectroscopic studies have suggested that U(V) can be stabilized via its incorporation into magnetite within the octahedral sites in a distorted uranate-like coordination, although the exact structural site has not been conclusively determined, and no information about U(V) stabilization in other Fe(II)/Fe(III) (oxyhydr)oxides (e.g., green rust) is currently available.[8,16,19] Theoretical simulations of incorporation of U into iron (oxyhydr)oxide minerals have provided information about the U(VI) and U(V) coordination environment when substituted for octahedrally coordinated Fe within the magnetite structure.[21,31] Recently, advances in spectroscopic techniques have also demonstrated that U(IV), U(V), and U(VI) can be distinguished using high-energy resolution fluorescence-detected-X-ray absorption near edge structure (HERFD-XANES) techniques.[19] Ultimately, if U(V) is incorporated into the structure of Fe(II)/Fe(III) (oxyhydr)oxides after U(VI) reduction, this could prevent disproportionation and lead to long-term immobilization of U(V). However, the pathway and mechanism of U(V) incorporation into magnetite and green rust are either poorly defined or yet to be determined.

Here, we synthesized both magnetite and green rust with U(VI) via a co-precipitation process. We then gained detailed molecular scale insights into the speciation and atomic scale mechanisms of incorporation of U within the mineral structures using state-of-the-art HERFD-XANES spectroscopy in combination with extended X-ray absorption fine structure (EXAFS) spectroscopy. Synchrotron analysis unequivocally confirmed the reduction of U(VI) to stabilized, octahedrally coordinated U(V), which is incorporated within both magnetite and green rust. This facile stabilization of U(V) within these bulk mineral phases may have important implications for the fate of U in engineered and natural environments where U(V) has typically been considered transient.

METHODS

Mineral Synthesis and Characterization. Uranium-bearing magnetite and green rust were synthesized using a direct co-precipitation method in experiments performed at room temperature in an anaerobic chamber.[32] In brief, solutions of 0.1 M $FeCl_2$, 0.2 M $FeCl_3$, 0.3 M HCl, and 0.0126 M U(VI)Cl_6 were mixed for 24 h before mineral precipitation was induced by introduction of the Fe(II)/Fe(III) solution into a N_2-sparged 28−30% (w/v) NH_4OH solution (pH 11) that was being continuously stirred over 15 min to a final pH of 9. This led to the instantaneous co-precipitation of the uranium-doped minerals. Four different starting Fe(II)/Fe(III) ratios were used to form magnetite and green rust:

$$x = \frac{\text{Fe(II)}}{\text{Fe(III)}} = 0.5,\ 0.6,\ 0.8,\ \text{or } 2.0$$

After reaction, the solid samples were analyzed by powder X-ray diffraction (XRD) and transmission electron microscopy (TEM) to characterize their structure, particle size, and morphology. The distribution of uranium within the iron (oxyhydr)oxides particles was determined using acid dissolution performed as a function of $[H^+]$ in solution.[33]

X-ray Absorption Spectroscopy (XAS). Uranium L_3 edge XAS spectra were recorded on wet mineral pastes at Diamond Light Source, beamline B18,[34] in a liquid N_2 cryostat in fluorescent mode using a Ge detector.[35] Analysis of the EXAFS spectra was performed in Artemis and Athena with details given in the Supporting Information.[36−40] U M_4 edge HERFD-XANES spectra were recorded at European Synchrotron Radiation Facility, beamline ID26,[41] through the use of an X-ray emission spectrometer[42,43] and analyzed using iterative transformation factor analysis[12,44] to determine the proportion of U(IV), U(V), and U(VI) in the samples.

RESULTS AND DISCUSSION

Co-precipitation experiments were performed to determine the speciation of uranium following co-precipitation with either magnetite or green rust. The Fe(II)/Fe(III) (oxyhydr)oxides were co-precipitated with U(VI) at starting Fe(II)/Fe(III) ratios of 0.5/0.6 to synthesize magnetite and 0.8/2.0 to synthesize green rust (Figure S1). Additionally, transmission electron microscopy showed the magnetite was nanoparticulate, with particle sizes ranging from 1 to 20 nm (Figure S2). Green rust was present as pseudohexagonal plates of approximately 50−600 nm, and energy dispersive X-ray analysis showed chloride was present, indicating green rust chloride formed (Figure S3).

Reduction of U(VI) to Stable U(V). Uranium M_4 edge HERFD-XANES spectra were used to determine the oxidation state of U associated with the Fe(II)/Fe(III) (oxyhydr)oxide phases (Figure 1).[19,45,46] The energy of the XANES peak

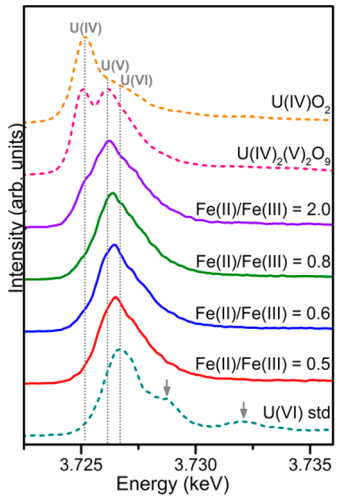

Figure 1. U M_4 edge HERFD-XANES of U co-precipitated with magnetite [Fe(II)/Fe(III) = 0.5 and 0.6] and green rust [Fe(II)/Fe(III) = 0.8 and 2.0] with standards U(IV)O_2,[46] U(IV)$_2$U(V)$_2O_9$,[46] and U(VI) adsorbed to ferrihydrite. Gray arrows indicate characteristic U(VI) features.

position showed a systematic decrease as the Fe(II)/Fe(III) ratio increased (Figure S4) from 3726.5 eV [at 0.5 Fe(II)/Fe(III)] to 3726.3 eV [at 2.0 Fe(II)/Fe(III)]. Comparison with the peak position of the U oxidation state standards [U(VI) = 3726.95 eV, U(V) = 3726.4 eV, and U(IV) = 3725.2 eV] suggests that U(V) dominated in all of the samples. Furthermore, there were no indications of the higher-energy peaks (3728.7 and 3732.0 eV) that are typical of U(VI). However, in the Fe(II)/Fe(III) = 2.0 spectra, the small shoulder on the low-energy side of the XANES spectrum confirms the presence of U(IV) (Figure 1). Iterative trans-

DOI: 10.1021/acs.estlett.7b00348
Environ. Sci. Technol. Lett. XXXX, XXX, XXX−XXX

formation factor analysis (ITFA) of the HERFD-XANES data identified the three main components present in the samples (Figure S5) and indicated that at Fe(II)/Fe(III) = 0.5−0.8, 87−96% of U was present as U(V), with the remainder being from U(VI) for Fe(II)/Fe(III) = 0.5 and U(IV) for Fe(II)/Fe(III) = 0.6 and 0.8 (Table S1). At Fe(II)/Fe(III) = 2.0, U(V) still dominated but the amount of U(IV) increased to approximately 28%. The U L_3 edge XANES also supports stabilization of U(V) with XANES edge positions for all the samples (17169.6−17171.2 eV) between those of U(VI) (17173.4 eV) and U(IV) (17170.3 eV). Additionally, shifts in the U L_3 edge XANES post-edge resonance features to a lower energy relative to that of the uranyl U(VI) standard indicate the formation of a uranate-like coordination[47] consistent with the reported U coordination within magnetite (Figure S6).[16,19]

Incorporation of U within Magnetite and Green Rust. U L_3 edge EXAFS spectra (Figure S7 and Table S2) were analyzed to determine the molecular scale speciation of U associated within the magnetite and green rust mineral phases. For U associated with magnetite [Fe(II)/Fe(III) = 0.5 and 0.6], the best fits confirm 4−4.5 oxygen backscatterers at 2.17(1) Å, indicative of uranate-like coordination,[8,13,15,16,19,47] which is consistent with our interpretation of the L_3 edge XANES spectra. The U−O coordination number is lower than would be predicted for an octahedral site (i.e., <6) because of the presence of a proportion of either U(IV)O_2 or U(VI) within the samples. The fitting of Fe shells to the EXAFS was then informed by assuming that incorporation of U into magnetite occurred by substituting U for Fe at an octahedrally coordinated Fe site. The fits confirmed the presence of two U−Fe shells at 3.20(2) and 3.72(2) Å for Fe(II)/Fe(III) = 0.5 and 3.15(2) and 3.69(3) Å for Fe(II)/Fe(III) = 0.6, showing a systematic and significant increase in the interatomic distance relative to the Fe−Fe distances in magnetite (2.97 and 3.48 Å, respectively[38]). At Fe(II)/Fe(III) = 0.6, the additional U−O and U−U backscattering shells observed at 2.42(2) and 3.89(2) Å, respectively, reflect the presence of U(IV) supporting the HERFD-XANES data, and assuming an error of ±1 on the coordination number, the proportions of U(IV) are within error [i.e., 4−20% U(IV)]. Finally, the presence of oxygen backscatterers at 1.81(2) and 2.43(2) Å in the fit for the Fe(II)/Fe(III) = 0.5 sample suggests a modest contribution from U(VI) in uranyl dioxygenyl coordination. This was confirmed by the ITFA analysis and has previously been attributed to U(VI) adsorbed to magnetite.[8,15]

For Fe(II)/Fe(III) = 0.8 and 2.0 samples, the U−O coordination environment in green rust showed differences when compared to the magnetite system, with U−O distances at approximately 1.90(6) and 2.17(1) Å again indicative of uranate-like coordination. Similar to the magnetite systems, additional U−O and U−U shells at 2.46(2) and 3.89(1) Å confirm the presence of U(IV)O_2, which is consistent with the HERFD-XANES analysis and previous studies.[25,48] Similar to the magnetite system, fitting of additional Fe shells was informed by the green rust structure and assumes direct substitution of octahedrally coordinated Fe by U. The best fits include six Fe atoms at 3.09(1) and 3.28(2) Å with an additional shell of four Fe atoms at 5.24(3) Å. These fits are consistent with the Fe−Fe distances in green rust, which are 3.19 and 5.52 Å, respectively. The dissolution experiments for the Fe(II)/Fe(III) = 0.5, 0.6, and 0.8 samples (Figure S8) show an initial release of 35−40% of U with minimal Fe dissolution, followed by congruent dissolution of U and Fe. This suggests that 60−65% of the U is distributed within the magnetite and/or green rust particles, with the remaining U being discrete U phases (i.e., UO_2) or near-surface-associated U(V)/U(VI).

Overall, the EXAFS and dissolution data confirm that U(V) is incorporated within octahedral sites in the Fe(II)/Fe(III) (oxyhydr)oxide phases in a uranate-like coordination environment. This is consistent with several recent experimental and theoretical reports showing U can directly substitute for octahedrally coordinated Fe in iron (oxyhydr)oxide mineral phases.[8,15,16,19,31] Our work extends these observations for the first time to systems in which U(V) is the dominant species during direct precipitation of both magnetite and green rust.

Mechanism of Incorporation of U(V) into Magnetite and Green Rust. Our results show that direct co-precipitation of U(VI) with magnetite and green rust leads to reduction of U(VI) to U(V) and subsequent stabilization within the bulk structure of both minerals. The stabilization of U(V) via incorporation into Fe(II)/Fe(III)-bearing iron (oxyhydr)oxides has been hypothesized in several systems,[8,15,16] with very recent work postulating U(V) stabilization via incorporation into magnetite.[19] For the current work, in both systems U(V) is incorporated into the mineral structures via direct substitution of U for octahedrally coordinated Fe. In magnetite, the average U(V)−O bond length is 2.17(1) Å [Fe(II)/Fe(III) = 0.5 and 0.6], consistent both with U(V) in uranate-like coordination[19,47] and with recent atomistic simulations that predict a U−O distance of 2.08 Å for this system.[19,31,49] The U−Fe interatomic distances derived from the EXAFS data (i.e., 3.15−3.20 and 3.69−3.72 Å) are consistent with those previously published.[19] The U−Fe distances are ≈0.2 Å longer than the Fe−Fe distances in magnetite, but the distance between the two Fe shells matches that of pure magnetite [≈0.5 Å (Table S2)]. Again these values are consistent with U(V) incorporation simulations for the first Fe shell (3.15 Å) in magnetite.[31] The reason for the increased interatomic distances is unlikely to be the size of the incorporated U(V) [the octahedral crystal radius of U(V) is 0.9 Å, and the radii for Fe(II) and Fe(III) are 0.92 and 0.785 Å, respectively]; rather, strengthened repulsive electrostatic interactions between U(V) and the Fe(II/III) atoms pushed the iron out.[31] The low coordination numbers of the U−Fe shells (2) relative to that of pure magnetite (6) are likely due to the nanoparticulate nature of magnetite, which leads to a proportion of the U being near-surface-associated.[50] This is consistent with the dissolution data that shows 35−40% of U is released with minimal Fe dissolution (Figure S8), suggesting this fraction is near-surface-associated U(V)/U(VI) and UO_2, with the remaining U distributed evenly throughout the particles. The presence of U(IV) at the (near) surface of the particles is likely due to the presence of Fe(II), which provides strong reducing conditions, resulting in the reduction of sorbed U to U(IV) surface complexes that can transform into UO_2 particles.

The incorporation of U(V) into green rust [Fe(II)/Fe(III) = 0.8 and 2.0] again occurs via direct substitution for octahedrally coordinated Fe within the sheet structure of the layered double hydroxide. In addition, the dissolution data indicate that 35−40% of U is present as a discrete phase or is near-surface-associated, which is consistent with the presence of UO_2 in the XAS, formed via the process stated above, and some near-surface-associated U(V). The EXAFS data indicate that the U(V) local coordination is different compared to that of magnetite (Figure S7). Indeed, the best fit for these samples confirmed two oxygens at ≈1.9 Å and a shell of four equatorial

DOI: 10.1021/acs.estlett.7b00348
Environ. Sci. Technol. Lett. XXXX, XXX, XXX−XXX

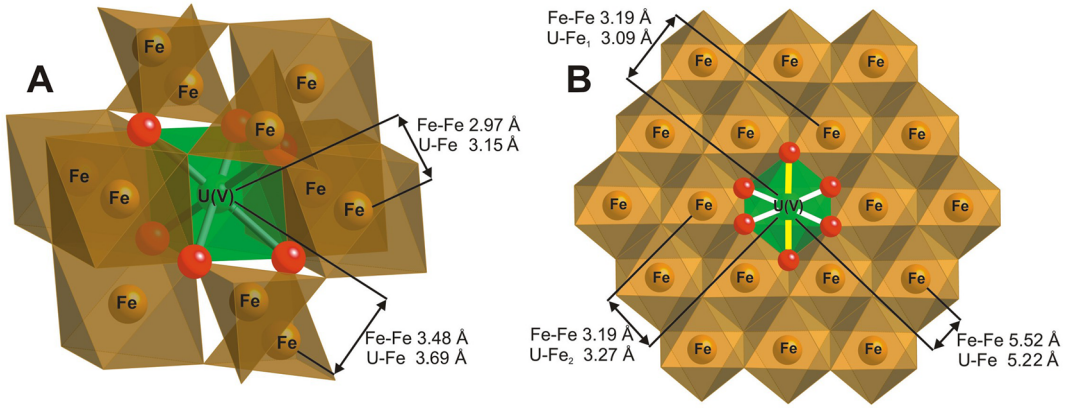

Figure 2. (A) Magnetite structure showing Fe−Fe distances[38] and U−Fe distances obtained from EXAFS at Fe(II)/Fe(III) = 0.6. (B) Green rust structures showing Fe−Fe distances[40] and U−Fe distances obtained from EXAFS at Fe(II)/Fe(III) = 2.0. Yellow lines indicate shorter U−O distances (1.9 Å), and white lines indicate longer U−O distances (2.17 Å).

oxygens at 2.17 Å, again consistent with a uranate-like coordination environment (Table S2). This difference in U(V)−O coordination relative to that of magnetite is presumably due to the layered structure of the green rust and similar to that observed for incorporation of U(V) into other layered iron (oxyhydr)oxides (i.e., lepidocrocite).[51] Here, incorporation of U(V) within isolated octahedral sheets evidently provides significantly less steric constraint on the U(V)−O octahedron relative to U(V) in the highly constrained cubic spinel structure of magnetite. The variation in the axial and equatorial U−O bond lengths in the U(V) incorporated within green rust clearly leads to local distortion of the green rust octahedral sheet and splitting of U−Fe distances relative to the Fe−Fe distances in green rust (Table S2). Overall, the best fit indicates three or four Fe−O octahedra adjacent to the short (1.9 Å) U−O axial oxygens and approximately two Fe−O octahedra adjacent to the long (2.17 Å) U−O equatorial oxygen distances (Figure 2). This is consistent with the U(V) being present in a distorted octahedral environment and is presumably due to the enhanced flexibility of the octahedral sheet in green rust compared to octahedral sites within cubic magnetite.

The novel incorporation of U(V) in green rust is in contrast to the results of previous sorption studies in which U(IV) surface complexes or $UO_{2(s)}$ was observed as the reaction end product.[25,48,52]

The observed energy shift of the U(V) M_4 edge HERFD-XANES main peak position (Figure 1) for different Fe(II)/Fe(III) ratios (Figure S4) from 3726.5 eV [Fe(II)/Fe(III) = 0.5] to 3726.3 eV [Fe(II)/Fe(III) = 2.0] may relate to the different strengths of the covalent bond between the U and neighboring atoms.[53] Electronic structure calculations (Figure S9) show a clear difference in the distribution of density of states for U incorporated into the octahedral site of magnetite relative to green rust. The hybridization between U f states and Fe d states above the Fermi level is much stronger for U incorporated into green rust than for U incorporated into magnetite. This may be associated with a stronger, more covalent, U bond in green rust compared to the U bond in the magnetite structure.

Mechanism of U(V) Stabilization. Our results suggest that U(V) incorporation during magnetite and green rust formation occurs via a two-step process (abstract graphic). First, we suggest that U(VI) is adsorbed to the surface of the growing Fe(II)/Fe(III) (oxyhydr)oxide nanoparticles and undergoes reduction to U(V) via one-electron transfer.[8] Second, during rapid crystal growth, the U(V), which is compatible with the Fe octahedral site in both magnetite[19] and green rust, becomes incorporated within the structure. These steps are consistent with those proposed for U(V) incorporation during goethite formation;[14] however, further research is required to determine the exact nature of each step in the process. Recent work has highlighted that disproportion of U(V) can occur on the magnetite surface, implying that stabilization of structural U(V) may occur only during rapid crystal growth.[10] Under these conditions, isolation of U(V) within the mineral structure may prevent its disproportionation to U(IV) and U(VI). Indeed, U(V) is reportedly stable in magnetite for up to 550 days, suggesting that incorporated U(V) may be stable over extended time periods.[15] Furthermore, steric constraints seem likely to favor U(V) stabilization in these systems as U(IV) strongly prefers larger coordination environments (e.g., n = 8).[8,13,20] Indeed, steric constraints may be the most crucial factor in stabilizing U(V) as both magnetite and green rust are electrically conductive,[54] and therefore, physical isolation of U(V) alone seems unlikely to prevent disproportionation.

Implications for U Speciation and the Fate of U in the Environment. Here, we have shown the reduction of U(VI) to U(V) followed by incorporation into both magnetite and green rust is the dominant process during the direct precipitation of these mineral phases. The potential for U(V) incorporation processes to be dominant in these environmentally relevant phases is certainly highlighted in this and other very recent work[19] and has important implications, which have not been fully explored, for understanding and predicting U mobility in engineered and natural environments. Clearly, the extent of incorporation of U(V) into Fe(II)/Fe(III) (oxyhydr)oxides forming under contaminated land and geodisposal conditions needs to be fully quantified. Incorporation of U(V) into mineral phases commonly present in contaminated environments may offer a more resilient species for oxidative remobilization compared to uraninite and adsorbed U(IV), which are readily oxidized to soluble U(VI) in many environmental systems.[16,55] The incorporation of U(V) into magnetite and green rust offers a promising prospect for optimizing its incorporation in a range of engineered settings, while the stability of U(V) in these systems clearly warrants further investigation.

DOI: 10.1021/acs.estlett.7b00348
Environ. Sci. Technol. Lett. XXXX, XXX, XXX−XXX

■ ASSOCIATED CONTENT

Supporting Information

The Supporting Information is available free of charge on the ACS Publications website at DOI: 10.1021/acs.estlett.7b00348.

Additional figures and tables showing XRD patterns, TEM images and EDS analyses, HERFD-XANES data and fitting results, EXAFS fitting parameters, dissolution data, and a description of the EXAFS fitting process (PDF)

■ AUTHOR INFORMATION

Corresponding Author

*E-mail: sam.shaw@manchester.ac.uk. Telephone: +44 (0)161 275 3826.

ORCID

Katherine Morris: 0000-0002-0716-7589

Gareth T. W. Law: 0000-0002-2320-6330

J. Frederick W. Mosselmans: 0000-0001-6473-2743

Samuel Shaw: 0000-0002-6353-5454

Present Address

#P.B.: Department of Civil and Environmental Engineering, University of Strathclyde, Glasgow G1 1XJ, United Kingdom.

Notes

The authors declare no competing financial interest.

■ ACKNOWLEDGMENTS

This work was supported by the STFC (ST/L502534/1), Env Rad Net (ST/K001787/1 and ST/N002474/1), and BIGRAD (NE/H007768/1). We thank both Diamond Light Source (DLS) (SP9621-2, SP10163-1, and SP12767-1) and European Synchrotron Radiation Facility (ESRF) (EV/192) for beam time. We thank Dr. Giannantonio Cibin, Dr. Steve Parry, and Richard Doull for their help during beam time at DLS, Dr. Sara Lafuerza for help during beam time at ESRF, Dr. John Waters for help with XRD, Dr. Heath Bagshaw for help with TEM, Ellen Winstanley for providing U(VI) HERFD-XANES data, and Dr. Carolyn Pearce for help with the mineral synthesis method.

■ REFERENCES

(1) Newsome, L.; Morris, K.; Lloyd, J. R. The biogeochemistry and bioremediation of uranium and other priority radionuclides. *Chem. Geol.* **2014**, *363*, 164−184.

(2) Moyce, E. B. A.; Rochelle, C.; Morris, K.; Milodowski, A. E.; Chen, X.; Thornton, S.; Small, J. S.; Shaw, S. Rock alteration in alkaline cement waters over 15 years and its relevance to the geological disposal of nuclear waste. *Appl. Geochem.* **2014**, *50*, 91−105.

(3) Gavrilescu, M.; Pavel, L. V.; Cretescu, I. Characterization and remediation of soils contaminated with uranium. *J. Hazard. Mater.* **2009**, *163* (2−3), 475−510.

(4) Bone, S. E.; Dynes, J. J.; Cliff, J.; Bargar, J. R. Uranium(IV) adsorption by natural organic matter in anoxic sediments. *Proc. Natl. Acad. Sci. U. S. A.* **2017**, *114* (4), 711.

(5) Ekstrom, A. Kinetics and Mechanism of the Disproportionation of Uranium(V). *Inorg. Chem.* **1974**, *13* (9), 2237−2241.

(6) Steele, H.; Taylor, R. J. A Theoretical Study of the Inner-Sphere Disproportionation Reaction Mechanism of the Pentavalent Actinyl Ions. *Inorg. Chem.* **2007**, *46* (16), 6311−6318.

(7) Ikeda, A.; Hennig, C.; Tsushima, S.; Takao, K.; Ikeda, Y.; Scheinost, A. C.; Bernhard, G. Comparative study of uranyl(VI) and -(V) carbonato complexes in an aqueous solution. *Inorg. Chem.* **2007**, *46* (10), 4212−4219.

(8) Ilton, E. S.; Boily, J. F.; Buck, E. C.; Skomurski, F. N.; Rosso, K. M.; Cahill, C. L.; Bargar, J. R.; Felmy, A. R. Influence of Dynamical Conditions on the Reduction of UVI at the Magnetite-Solution Interface. *Environ. Sci. Technol.* **2010**, *44*, 170−176.

(9) Ilton, E. S.; Haiduc, A.; Cahill, C. L.; Felmy, A. R. Mica Surfaces Stabilize Pentavalent Uranium. *Inorg. Chem.* **2005**, *44* (9), 2986−2988.

(10) Yuan, K.; Renock, D.; Ewing, R. C.; Becker, U. Uranium reduction on magnetite: Probing for pentavalent uranium using electrochemical methods. *Geochim. Cosmochim. Acta* **2015**, *156*, 194−206.

(11) Yuan, K.; Ilton, E. S.; Antonio, M. R.; Li, Z.; Cook, P. J.; Becker, U. Electrochemical and Spectroscopic Evidence on the One-Electron Reduction of U(VI) to U(V) on Magnetite. *Environ. Sci. Technol.* **2015**, *49* (10), 6206−6213.

(12) Tsarev, S.; Collins, R. N.; Fahy, A.; Waite, T. D. Reduced Uranium Phases Produced from Anaerobic Reaction with Nanoscale Zerovalent Iron. *Environ. Sci. Technol.* **2016**, *50* (5), 2595−2601.

(13) Ilton, E. S.; Pacheco, J. S. L.; Bargar, J. R.; Shi, Z.; Liu, J.; Kovarik, L.; Engelhard, M. H.; Felmy, A. R. Reduction of U(VI) Incorporated in the Structure of Hematite. *Environ. Sci. Technol.* **2012**, *46*, 9428−9436.

(14) Massey, M. S.; Lezama-Pacheco, J. S.; Jones, M. E.; Ilton, E. S.; Cerrato, J. M.; Bargar, J. R.; Fendorf, S. Competing retention pathways of uranium upon reaction with Fe(II). *Geochim. Cosmochim. Acta* **2014**, *142* (1), 166−185.

(15) Huber, F.; Schild, D.; Vitova, T.; Rothe, J.; Kirsch, R.; Schäfer, T. U(VI) removal kinetics in presence of synthetic magnetite nanoparticles. *Geochim. Cosmochim. Acta* **2012**, *96*, 154−173.

(16) Marshall, T. A.; Morris, K.; Law, G. T. W.; Mosselmans, J. F. W.; Bots, P.; Roberts, H.; Shaw, S. Uranium fate during crystallization of magnetite from ferrihydrite in conditions relevant to the disposal of radioactive waste. *Mineral. Mag.* **2015**, *79* (6), 1265−1274.

(17) Boland, D. D.; Collins, R. N.; Payne, T. E.; Waite, T. D. Effect of Amorphous Fe(III) Oxide Transformation on the Fe(II)-Mediated Reduction of U(VI). *Environ. Sci. Technol.* **2011**, *45*, 1327−1333.

(18) Boland, D. D.; Collins, R. N.; Glover, C. J.; Payne, T. E.; Waite, T. D. Reduction of U(VI) by Fe(II) during the Fe(II)-Accelerated Transformation of Ferrihydrite. *Environ. Sci. Technol.* **2014**, *48* (16), 9086−9093.

(19) Pidchenko, I.; Kvashnina, K. O.; Yokosawa, T.; Finck, N.; Bahl, S.; Schild, D.; Polly, R.; Bohnert, E.; Rossberg, A.; Göttlicher, J.; et al. Uranium Redox Transformations after U(VI) Coprecipitation with Magnetite Nanoparticles. *Environ. Sci. Technol.* **2017**, *51*, 2217−2225.

(20) Skomurski, F. N.; Ilton, E. S.; Engelhard, M. H.; Arey, B. W.; Rosso, K. M. Heterogeneous reduction of U6+ by structural Fe2+ from theory and experiment. *Geochim. Cosmochim. Acta* **2011**, *75* (22), 7277−7290.

(21) Kerisit, S.; Bylaska, E. J.; Massey, M. S.; McBriarty, M. E.; Ilton, E. S. Ab initio molecular dynamics of uranium incorporated in goethite (α-FeOOH): Interpretation of X-ray absorption spectroscopy of trace polyvalent metals. *Inorg. Chem.* **2016**, *55* (22), 11736−11746.

(22) Refait, P.; Genin, J. M. R. The oxidation of ferrous hydroxide in chloride-containing aqueous media and pourbaix diagrams of green rust one. *Corros. Sci.* **1993**, *34* (5), 797−819.

(23) Byrne, J. M.; Telling, N. D.; Coker, V. S.; Pattrick, R. A. D.; van der Laan, G.; Arenholz, E.; Tuna, F.; Lloyd, J. R. Control of nanoparticle size, reactivity and magnetic properties during the bioproduction of magnetite by Geobacter sulfurreducens. *Nanotechnology* **2011**, *22* (45), 455709.

(24) O'Loughlin, E. J.; Larese-Casanova, P.; Scherer, M.; Cook, R. Green Rust Formation from the Bioreduction of γ−FeOOH (Lepidocrocite): Comparison of Several Shewanella Species. *Geomicrobiol. J.* **2007**, *24* (Ii), 211−230.

(25) Dodge, C. J.; Francis, A. J.; Gillow, J. B.; Halada, G. P.; Eng, C.; Clayton, C. R. Association of uranium with iron oxides typically formed on corroding steel surfaces. *Environ. Sci. Technol.* **2002**, *36* (16), 3504−3511.

DOI: 10.1021/acs.estlett.7b00348
Environ. Sci. Technol. Lett. XXXX, XXX, XXX−XXX

(26) Tremaine, P. R.; LeBlanc, J. C. The solubility of magnetite and the hydrolysis and oxidation of Fe2+ in water to 300°C. *J. Solution Chem.* **1980**, *9* (6), 415−442.
(27) Musić, S.; Ristić, M. Adsorption of trace elements or radionuclides on hydrous iron oxides. *J. Radioanal. Nucl. Chem.* **1988**, *120* (2), 289−304.
(28) Latta, D. E.; Mishra, B.; Cook, R. E.; Kemner, K. M.; Boyanov, M. I. Stable U(IV) complexes form at high-affinity mineral surface sites. *Environ. Sci. Technol.* **2014**, *48* (3), 1683−1691.
(29) Scott, T. B.; Allen, G. C.; Heard, P. J.; Randell, M. G. Reduction of U(VI) to U(IV) on the surface of magnetite. *Geochim. Cosmochim. Acta* **2005**, *69* (24), 5639−5646.
(30) Wang, Z.; Ulrich, K.-U.; Pan, C.; Giammar, D. E. Measurement and Modeling of U(IV) Adsorption to Metal Oxide Minerals. *Environ. Sci. Technol. Lett.* **2015**, *2* (8), 227−232.
(31) Kerisit, S.; Felmy, A. R.; Ilton, E. S. Atomistic simulations of uranium incorporation into iron (hydr)oxides. *Environ. Sci. Technol.* **2011**, *45* (7), 2770−2776.
(32) Pearce, C. I.; Qafoku, O.; Liu, J.; Arenholz, E.; Heald, S. M.; Kukkadapu, R. K.; Gorski, C. A.; Henderson, C. M. B.; Rosso, K. M. Synthesis and properties of titanomagnetite (Fe 3-xTi xO 4) nanoparticles: A tunable solid-state Fe(II/III) redox system. *J. Colloid Interface Sci.* **2012**, *387* (1), 24−38.
(33) Doornbusch, B.; Bunney, K.; Gan, B. K.; Jones, F.; Gräfe, M. Iron oxide formation from FeCl2 solutions in the presence of uranyl (UO22+) cations and carbonate rich media. *Geochim. Cosmochim. Acta* **2015**, *158*, 22−47.
(34) Burke, I. T.; Mosselmans, J. F. W.; Shaw, S.; Peacock, C. L.; Benning, L. G.; Coker, V. S. Impact of the Diamond Light Source on Research in Earth and Environmental Sciences: Current Work and Future Perspectives. *Philos. Trans. R. Soc., A* **2015**, *373*, 20130151.
(35) Dent, A. J.; Cibin, G.; Ramos, S.; Smith, A. D.; Scott, S. M.; Varandas, L.; Pearson, M. R.; Krumpa, N. A.; Jones, C. P.; Robbins, P. E. B18: A core XAS spectroscopy beamline for Diamond. *J. Phys.: Conf. Ser.* **2009**, *190* (1), 012039.
(36) Ravel, B.; Newville, M. ATHENA, ARTEMIS, HEPHAESTUS: Data analysis for X-ray absorption spectroscopy using IFEFFIT. *J. Synchrotron Radiat.* **2005**, *12*, 537−541.
(37) Bannister, M. J.; Taylor, J. C. The crystal structure and anisotropic thermal expansion of β-uranyl dihydroxide, $UO_2(OH)_2$. *Acta Crystallogr., Sect. B: Struct. Crystallogr. Cryst. Chem.* **1970**, *26* (11), 1775−1781.
(38) Fleet, M. E. The structure of magnetite. *Acta Crystallogr., Sect. B: Struct. Crystallogr. Cryst. Chem.* **1981**, *37* (4), 917−920.
(39) Barrett, S.; Jacobson, A. J.; Tofield, B. C.; Fender, B. E. F. The Preparation and Structure of Barium Uranium Oxide BaUO3+X. *Acta Crystallogr., Sect. B: Struct. Crystallogr. Cryst. Chem.* **1982**, *38*, 2775−2781.
(40) Simon, L.; François, M.; Refait, P.; Renaudin, G.; Lelaurain, M.; Génin, J. M. R. Structure of the Fe(II-III) layered double hydroxysulphate green rust two from Rietveld analysis. *Solid State Sci.* **2003**, *5* (2), 327−334.
(41) Gauthier, C.; Solé, V. A.; Signorato, R.; Goulon, J.; Moguiline, E. The ESRF beamline ID26: X-ray absorption on ultra dilute sample. *J. Synchrotron Radiat.* **1999**, *6*, 164−166.
(42) Glatzel, P.; Bergmann, U. High resolution 1s core hole X-ray spectroscopy in 3d transition metal complexes - Electronic and structural information. *Coord. Chem. Rev.* **2005**, *249* (1−2), 65−95.
(43) Kvashnina, K. O.; Scheinost, A. C. A Johann-type X-ray emission spectrometer at the Rossendorf beamline. *J. Synchrotron Radiat.* **2016**, *23* (3), 836−841.
(44) Rossberg, A.; Ulrich, K. U.; Weiss, S.; Tsushima, S.; Hiemstra, T.; Scheinost, A. C. SI: Identification of uranyl surface complexes on ferrihydrite: Advanced EXAFS data analysis and CD-music modeling. *Environ. Sci. Technol.* **2009**, *43* (5), 1400−1406.
(45) Vitova, T.; Kvashnina, K. O.; Nocton, G.; Sukharina, G.; Denecke, M. A.; Butorin, S. M.; Mazzanti, M.; Caciuffo, R.; Soldatov, A.; Behrends, T.; Geckeis, H. High energy resolution x-ray absorption spectroscopy study of uranium in varying valence states. *Phys. Rev. B: Condens. Matter Mater. Phys.* **2010**, *82* (23), 235118.
(46) Kvashnina, K. O.; Butorin, S. M.; Martin, P.; Glatzel, P. Chemical state of complex uranium oxides. *Phys. Rev. Lett.* **2013**, *111*, 25.
(47) Soldatov, A. V.; Lamoen, D.; Konstantinović, M. J.; Van den Berghe, S.; Scheinost, A. C.; Verwerft, M. Local structure and oxidation state of uranium in some ternary oxides: X-ray absorption analysis. *J. Solid State Chem.* **2007**, *180* (1), 54−61.
(48) O'Loughlin, E. J.; Kelly, S. D.; Cook, R. E.; Csencsits, R.; Kemner, K. M. Reduction of uranium(VI) by mixed iron(II)/iron(III) hydroxide (green rust): formation of UO2 nanoparticles. *Environ. Sci. Technol.* **2003**, *37* (4), 721−727.
(49) Shuller-Nickles, L.; Bender, W.; Walker, S.; Becker, U. Quantum-Mechanical Methods for Quantifying Incorporation of Contaminants in Proximal Minerals. *Minerals* **2014**, *4* (3), 690−715.
(50) Marshall, T. A.; Morris, K.; Law, G. T. W.; Mosselmans, J. F. W.; Bots, P.; Parry, S. A.; Shaw, S. Incorporation and retention of 99-Tc(IV) in magnetite under high pH conditions. *Environ. Sci. Technol.* **2014**, *48* (20), 11853−11862.
(51) McBriarty, M. E.; Soltis, J. A.; Kerisit, S.; Qafoku, O.; Bowden, M. E.; Bylaska, E. J.; De Yoreo, J. J.; Ilton, E. S. Trace Uranium Partitioning in a Multiphase Nano-FeOOH System. *Environ. Sci. Technol.* **2017**, *51* (9), 4970−4977.
(52) Latta, D. E.; Boyanov, M. I.; Kemner, K. M.; O'Loughlin, E. J.; Scherer, M. Reaction of Uranium(VI) with Green Rusts: Effect of Interlayer Anion. *Curr. Inorg. Chem.* **2015**, *5*, 156−168.
(53) Neidig, M. L.; Clark, D. L.; Martin, R. L. Covalency in f-element complexes. *Coord. Chem. Rev.* **2013**, *257* (2), 394−406.
(54) Hubbard, C. G.; West, L. J.; Rodriguez-Blanco, J. D.; Shaw, S. Laboratory study of spectral induced polarization responses of magnetite — Fe2+ redox reactions in porous media. *Geophysics* **2014**, *79* (1), D21−D30.
(55) Finch, R. J.; Ewing, R. C. The corrosion of uraninite under oxidizing conditions. *J. Nucl. Mater.* **1992**, *190* (C), 133−156.

DOI: 10.1021/acs.estlett.7b00348
Environ. Sci. Technol. Lett. XXXX, XXX, XXX−XXX